Time-Resolved Resonance Raman Observation of the Dimerization of Didehydroazepines in Solution

Jiadan Xue,[†] Yong Du,[†] Yung Ping Chuang,[†] David Lee Phillips,*[,†] Jin Wang,[‡] Calvin Luk,[‡] Christopher M. Hadad,*[,‡] and Matthew S. Platz*[,‡]

Department of Chemistry, The University of Hong Kong, Pokfulam Road, Hong Kong S.A.R., People's Republic of China, and Department of Chemistry, The Ohio State University, 100 West 18th Avenue, Columbus, Ohio 43210

Received: September 8, 2007; In Final Form: November 21, 2007

Time-resolved resonance Raman (TR^3) studies of the photochemistry of phenyl azide, 3-hyroxyphenyl azide, 3-methoxyphenyl azide and 3-nitrophenyl azide in acetonitrile:water solutions is reported. After photolysis of these four aryl azides in room temperature solutions, only one species was observed in the TR^3 spectra for each azide, respectively at the probe wavelengths employed in the TR^3 experiments. The species observed after photolysis of 3-nitrophenyl azide was assigned to 3,3′-dinitroazobenzene, an azo compound formed from the dimerization reaction of triplet 3-nitrophenylnitrene. In contrast, the species observed after photolysis of phenyl azide, 3-hydroxyphenyl azide and 3-methoxyphenyl azide were tentatively assigned to intermediates formed from the dimerization of didehydroazepines that are produced from the ring expansion reaction of the respective singlet arylnitrene. To our knowledge, this is the first time-resolved vibrational spectroscopic observation of the dimerization reaction of didehydroazepines in solution. In addition, these are the first resonance Raman spectra reported for dimers formed from didehydroazepines. We briefly discuss the structures, properties and chemical reactivity of the dimer species observed in the TR^3 spectra and possible implications for the photochemistry of aryl azides.

Introduction

Photolysis of aryl azides in solution usually proceeds by extrusion of a nitrogen molecule and the release of a singlet arylnitrene intermediate that has a very short lifetime (0.1−100 ns) at ambient temperature.[1] The singlet arylnitrene mainly undergoes two reaction pathways where one pathway is intersystem crossing (ISC) to form a triplet arylnitrene, which subsequently undergoes dimerization to form a stable azo compound, and the second pathway is a ring expansion reaction to give 1,2-didehydroazepine (cyclic ketenimine) intermediates that may undergo further reactions.[1] Some 1,2-didehydroazepines were found to be reactive intermediates generated in typical photoaffinity labeling experiments utilizing aryl azides in aqueous solution.[2] A very few singlet arylnitrenes are protonated in neutral water to form arylnitrenium ions.[3] This chemistry and the reaction mechanisms for singlet arylnitrenes have been well studied.[4−30] However, there are not many reports of time-resolved vibrational spectroscopic studies of singlet arylnitrenes in room temperature solution. Several singlet arylnitrenes have been studied using time-resolved infrared (TRIR) spectroscopy[8,9,28] and time-resolved resonance Raman (TR^3) spectroscopy[27,29] in organic solvents. A typical 1,2-didehydroazepine intermediate is produced in organic solvents within 1−10 ns through a benzazirine intermediate whose lifetime is as short as or shorter than that of the singlet arylnitrene. The 1,2-didehydroazepine intermediate has typical lifetimes of about 1 ms in dilute solutions and can be trapped by nucleophiles such as diethylamine and pyridine. Without any trapping agent present in the solution, 1,2-didehydroazepines are reported to form polymeric tars,[31] but the structures of theses tars and how they are formed are not clear. In highly dilute solution, 1,2-didehydroazepine can equilibrate with the corresponding singlet nitrene, which eventually will relax to form the lower energy triplet nitrene.

In this paper, we report a nanosecond TR^3 study of reactions that follow the photolysis of phenyl azide (PAz) and a range of *meta* substituted phenyl azides including 3-hydroxyphenyl azide (OHPAz), 3-methoxyphenyl azide (MeOPAz) and 3-nitrophenyl azide (NitroPAz) in room temperature solutions. During these TR^3 experiments, only one species was observed for each azide, respectively. For the NitroPAz, the observed species was an azo compound with a distinctly different structure from the other three species observed with the other precursors. The results of the concentration dependence and the laser power dependence experiments demonstrated that the intermediates produced by photolysis of the PAz, OHPAz and MeOPAz also had dimeric structures, but these are thought to arise from the corresponding 1,2-didehydroazipines (Scheme 1) on the basis of previous laser flash photolysis studies.[2a] Density functional theory (DFT) calculations were used in this paper to predict the Raman spectra of these dimer intermediates. Upon comparison of the calculated Raman spectra to those obtained by the TR^3 experiments, the specific structures of these dimers were predicted. To our knowledge, this is the first time vibrational spectroscopy has been employed to characterize the dimeric intermediates formed from 1,2-didehydroazepines. We discuss the structures, properties and chemical reactivity of the dimer intermediates produced from 1,2-didehydroazepines and the potential implications for the production of polymeric tars and the chemical reactivity of

* Authors to whom correspondence should be addressed.E-mail: D.L.P., phillips@hkucc.hku.hk; C.M.H., hadad@chemistry.ohio-state.edu; M.S.P., platz.1@osu.edu.
[†] The University of Hong Kong.
[‡] The Ohio State University.

10.1021/jp077215g CCC: $40.75
Published on Web 01/29/2008

SCHEME 1

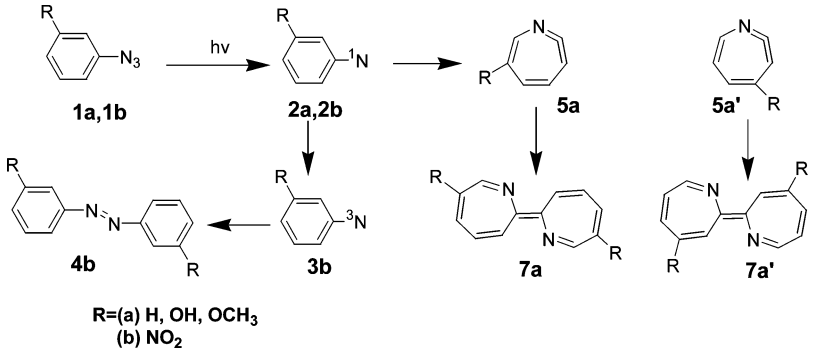

Azirine intermediates between singlet nitrene and didehydroazepine have not been shown in order to economize space.

1,2-didehydroazepines observed to be reactive intermediates generated in typical photoaffinity labeling experiments utilizing aryl azides.

Experimental and Computational Methods

Samples of PAz, OHPAz, MeOPAz and NitroPAz were synthesized according to literature methods.[32] Spectroscopic grade acetonitrile and deionized water were used in preparing sample solutions. Samples of the four phenyl azides were prepared with concentrations of ~3 mM in pure acetonitrile and/or water:acetonitrile (50:50 by volume) and/or water:acetonitrile (95:5 by volume) solvents for nanosecond TR^3 experiments. An authentic sample of azobenzene was purchased from Aldrich (>98%) and used as received in the 341.5 nm resonance Raman experiment with a sample concentration of about 1 mM in acetonitrile solvent. An authentic sample of 3,3′-dinitroazobenzene was synthesized following a literature method,[32] and used in the 341.5 nm resonance Raman experiment with a sample concentration of about 1 mM in acetonitrile solvent.

The experimental apparatus and methods used for the nanosecond time-resolved resonance Raman (ns-TR^3) and resonance Raman experiments have been detailed elsewhere,[27,33−36] so only a brief account will be given here. The fourth harmonic of a Nd:YAG nanosecond pulsed laser system providing the 266 nm pump laser pulse and the 341.5 nm probe laser pulse from the second Stokes hydrogen Raman shifted line of the 266 nm fourth harmonic were employed in the ns-TR^3 experiments. The ns-TR^3 experiments utilized two Nd:YAG lasers electronically synchronized to each other by a pulse delay generator used to control the relative timing of the two lasers. A fast photodiode whose output was displayed on a 500 MHz oscilloscope was used to measure the relative timing of the pump and probe pulses with the jitter between the pump and probe pulses observed to be <5 ns. The laser beams were loosely focused onto a flowing liquid stream of sample using a near collinear geometry and the scattered Raman light was collected employing reflective optics and a backscattering geometry. The collected Raman light was imaged through a depolarizer mounted on the entrance of a monochromator that dispersed the light onto a liquid nitrogen cooled CCD detector that collected the Raman signal for 30−60 s before reading out to an interfaced PC computer. About 10−20 of these scans were summed to obtain the resonance Raman spectrum. The TR^3 spectra were determined by subtracting the pump−probe spectrum at negative 100 ns from pump−probe spectra acquired at positive time delays to remove the solvent and precursor Raman bands. The known wavenumbers of the acetonitrile Raman bands were used to calibrate the wavenumber of the TR^3 spectra to an absolute accuracy of about ±3 cm^{-1}. A Lorentzian function was used to integrate the relevant Raman bands in the TR^3 spectra to find their areas and determine the decay and growth kinetics of the species observed in the TR^3 experiments. During the TR^3 experiments no noticeable degradation was observed for the sample by UV/vis absorption spectroscopy.

All of the density functional theory calculations presented here made use of the Gaussian 98 program suite[37] operated on the High Performance Computing cluster installed at either the University of Hong Kong or the Ohio Supercomputer Center. Complete geometry optimization and vibrational frequency calculations were done analytically using the B3LYP method with the 6-31G* basis set for the species of interest. A Lorentzian function with a 20 cm^{-1} bandwidth was employed with the calculated Raman vibrational frequencies and relative intensities to find the B3LYP/6-31G* calculated Raman spectra presented here.

Results and Discussion

A. Time-Resolved Resonance Raman Spectra Acquired after 266 nm Photolysis of NitroPAz, PAz, OHPAz and MeOPAz. Figures 1 and 2 display the ns-TR^3 spectra acquired at various time-delays after photolysis of ~3 mM NitroPAz, PAz, OHPAz and MeOPAz in a water:acetonitrile (50:50) by

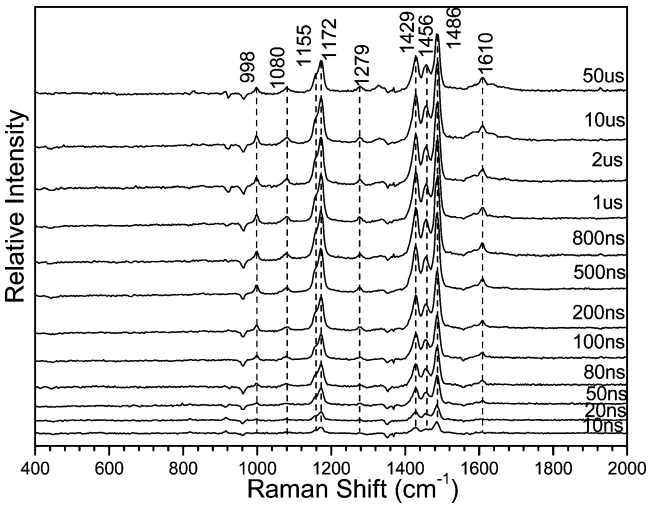

Figure 1. TR^3 spectra obtained using a 341.5 nm probe wavelength after 266 nm photolysis of ~3 mM NitroPAz in a water:acetonitrile (50:50) solution. The time delays between the pump (266 nm) and probe (341.5 nm) laser beams are shown to the right of each spectrum and the Raman shifts of selected bands are presented at the top of the 50 μs spectrum. See text for more details.

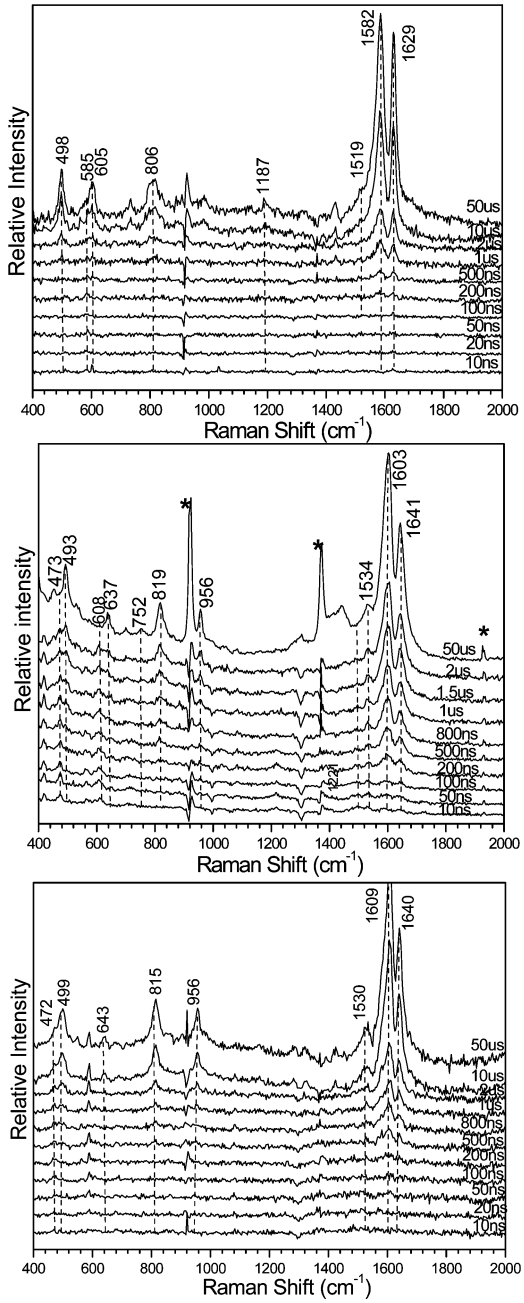

Figure 2. TR^3 spectra obtained using a 341.5 nm probe wavelength after 266 nm photolysis of ~3 mM PAz (top), OHPAz (middle) and MeOPAz (bottom) in a water:acetonitrile (50:50) solution. The time delays between the pump (266 nm) and probe (341.5 nm) laser beams are shown to the right of each spectrum and the Raman shifts of selected bands are presented at the top of the 50 μs spectra. See text for more details.

volume solution. The time-delays between the pump (266 nm) and probe (341.5 nm) laser beams are shown to the right of each spectrum and the Raman shifts of selected bands are presented at the top of the spectra. The TR^3 spectra in Figure 1 show that only one species can be observed from 10 ns to 50 μs by photolysis of NitroPAz, and this species has its strongest Raman bands at 1429, 1456 and 1486 cm^{-1} in the region from 1400 to 1500 cm^{-1}.

The spectra of Figure 1 are significantly different from those in Figure 2, produced by photolysis of PAz, OHPAz and MeOPAz, respectively. Inspection of Figure 2 shows that only one species is formed for each azide solution on the time scale examined here, and these three species have their two strongest Raman bands at around 1600 cm^{-1} accompanied by some moderate Raman bands at ~500, ~800 and ~1500 cm^{-1}. In addition, the Raman bands in Figure 2 at early time delays (before 500 ns), compared to those recorded 50 μs post photolysis, are not very strong, which indicates these species were formed with time constants on the microsecond time scale that is much slower than that for the species observed in Figure 1. Examination of the 50 μs spectra in Figure 2 shows that these three species have very similar Raman patterns for the strongest Raman bands at 1582, 1603 and 1609 cm^{-1} for the species obtained after photolysis of PAz, OHPAz and MeOPAz, and the second strongest Raman bands at 1629, 1641 and 1640 cm^{-1}, respectively, and some moderate intensity Raman bands at 498, 806 and 1519 cm^{-1} for the species obtained after photolysis of PAz compared to 493, 819 and 1534 cm^{-1} for the species obtained after photolysis of OHPAz and 499, 815 and 1530 cm^{-1} for the species obtained after photolysis of MeOPAz. This similarity suggests that these three species obtained after photolysis of PAz, OHPAz and MeOPAz have a similar chromophore and structure. There are also some small frequency shifts that appear to be due to the substituent effects of the 3-hydroxy and 3-methoxy groups.

The intermediate species observed in Figure 2 are insensitive to oxygen and have lifetimes of more than one hundred microseconds. An overview of the TR^3 spectra with more late time delays obtained after photolysis of OHPAz in a water:acetonitrile (50:50) solution are displayed in Figure 1S of the Supporting Information. Figures 2S−6S in the Supporting Information display the TR^3 spectra obtained after 266 nm photolysis of PAz, OHPAz and MeOPAz in acetonitrile and water:acetonitrile (95:5) solutions. Similar Raman spectra were observed after photolysis of these three azides in acetonitrile and water:acetonitrile (50:50) solutions only with modest variations that the strongest Raman bands in water:acetonitrile (50:50) shift down 3−9 cm^{-1} in acetonitrile, which can be accounted for by the hydrogen-bonding effects in aqueous solution. The similarities in the Raman spectra and the formation rates suggest that the same species were formed in acetonitrile and in mixed aqueous solution after photolysis of PAz, OHPAz and MeOPAz, respectively. This rules out an arylnitrenium ion assignment as this species cannot form in acetonitrile.

Azide concentration dependence and excitation power dependence experiments were performed to study the formation mechanism of the species observed in Figures 1 and 2. Figure 3 displays plots of the integrated areas for the strongest Raman band at 1486 cm^{-1} for the species obtained after photolysis of NitroPAz in a water:acetonitrile (50:50) solution as a function of time delays from 0 ns to 2 μs with two different azide concentrations (1 and 4 mM) and pump laser powers, in which the power density of the large power pump is more than twice that of the small power pump. Under the same experimental conditions, the species' growth can be fitted with time constants of 239 ns in the high concentration solution with low power, 243 ns in low concentration solution with low power and 80 ns in the high concentration solution with high power. This excitation power dependence and azide concentration independence behavior of the formation rates of the species obtained after photolysis of NitroPAz demonstrate that this species arises not from the reaction of the intermediate with azide precursor but probably from the dimerization of two intermediates.

Figure 4 displays plots of the integrated areas for the strongest Raman band at 1582 cm^{-1} for the species obtained after photolysis of phenyl azide in acetonitrile with two different azide concentrations as a function of time delays from 10 ns to 1000

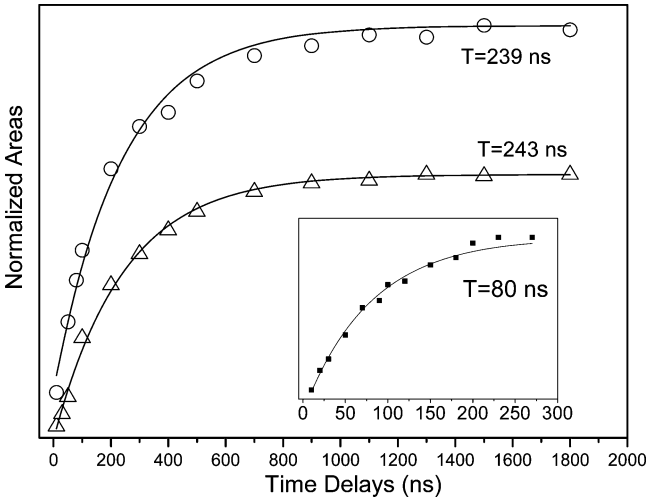

Figure 3. Plots of the integrated areas for the 1486 cm^{-1} Raman band for the species obtained after photolysis of NitroPAz in a water: acetonitrile (50:50) solution as a function of time delays with high azide concentration and low power (open circles), low azide concentration and low power (open triangles) and high azide concentration and high power (inset, solid squares). The data were fit to simple exponential growth functions as shown by the curves in the figures. Each of the kinetic curves was normalized to the largest Raman band intensity over the 10 ns to 2 μs time scale. The time constants for the best fit exponential kinetics are indicated next to the appropriate curves. See text for more details.

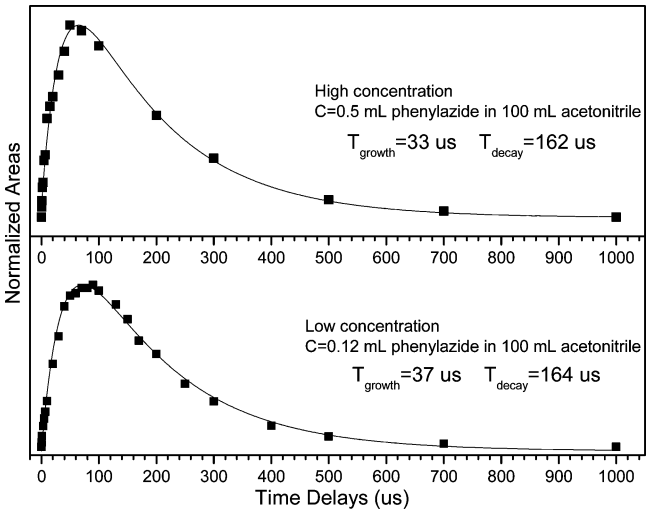

Figure 4. Plots of the integrated areas for the 1582 cm^{-1} Raman band for the species obtained after photolysis of PAz in acetonitrile with high azide concentration (top) and low azide concentration (bottom) as a function of time delays. The data were fit to simple exponential growth and decay functions as shown by the curves in the figures. Each of the kinetic curves was normalized to the largest Raman band intensity over the 10 ns to 1000 μs time scale. The time constants for the best fit exponential kinetics are indicated next to the appropriated curves. See text for more details.

μs. Under the same experimental conditions, the species' growth and decay in the high concentration (0.5 mL of sample in 100 mL of acetonitrile) and the low concentration (0.12 mL of sample in 100 mL of acetonitrile) solutions can be fitted with time constants of 33 and 162 μs in the high concentration solution compared to 37 and 164 μs in the low concentration solution for the growth and the decay of the species, respectively. This resemblance in the rise time of the species, despite the different concentrations of azide precursor, demonstrates that the species observed in TR^3 spectra of Figure 2 are not produced by the reaction of intermediates with the azide precursors.

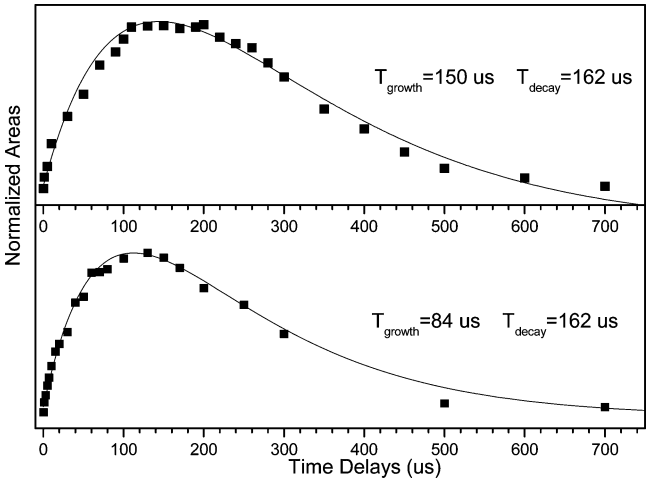

Figure 5. Plots of the integrated areas for the 1582 cm^{-1} Raman band for the species obtained after photolysis of PAz in acetonitrile using a small pump power (top) and a large pump power (bottom) as a function of the time delays. The data were fit to simple exponential growth and decay functions as shown by the curves in the figures. Each of the kinetic curves was normalized to the largest Raman band intensity over the 10 ns to 700 μs time scale. The time constants for the best fit exponential kinetics are indicated next to the appropriate curves. See text for more details.

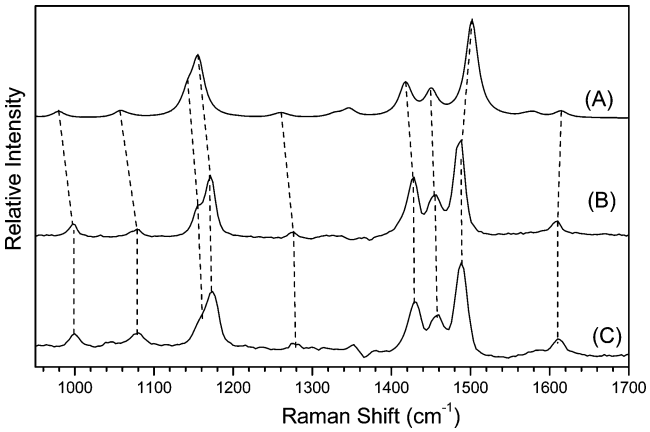

Figure 6. Comparison of (B) the experimental 50 μs TR^3 spectrum from Figure 1 obtained after photolysis of NitroPAz in a water: acetonitrile (50:50) solution to (A) the B3LYP/6-31G* calculated normal Raman spectra for 3,3′-dinitroazobenzene and (C) 341.5 nm resonance Raman spectrum of an authentic sample of 3,3′-dinitroazobenzene compound using a synthetic method. The calculated relative Raman intensities were convoluted with a Lorentzian function. See text and Table 1S for more details.

Different powers for the pump laser were also used to study the species observed in the TR^3 spectra of Figure 2. Figure 5 displays plots of the integrated areas for the characteristic Raman band at 1582 cm^{-1} for the species obtained by photolysis of phenyl azide in acetonitrile using small and large pump powers as a function of time delays from the 10 ns to 700 μs time scale, in which the power density of the large power pump is nearly twice that of the small power pump. When the other experimental conditions are the same, the fitted time constants for the growth of the species are significantly different for the formation time of these species, which are 150 μs using low pump power and 84 μs using the large power pump, indicating it is possible that the species observed in the TR^3 spectra of Figures 2 are produced by the reaction of these intermediates with themselves.

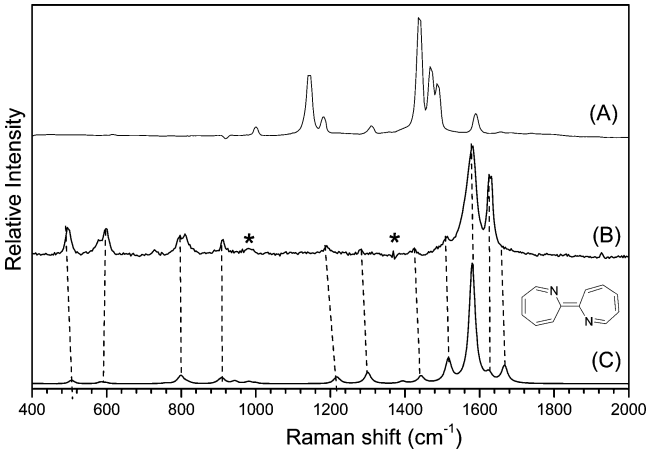

Figure 7. Comparison of (B) the experimental 50 μs TR^3 spectrum obtained after photolysis of PAz in a water:acetonitrile (50:50) solution to (A) the 341.5 nm resonance Raman spectrum of an authentic compound of azobenzene, and (C) the B3LYP/6-31G* calculated normal Raman spectrum for the DDA dimer **h** whose structure is displayed next to the calculated spectrum. Star symbols mark solvent-subtraction artifacts, stray-light and ambient-light artifacts. See text for more details.

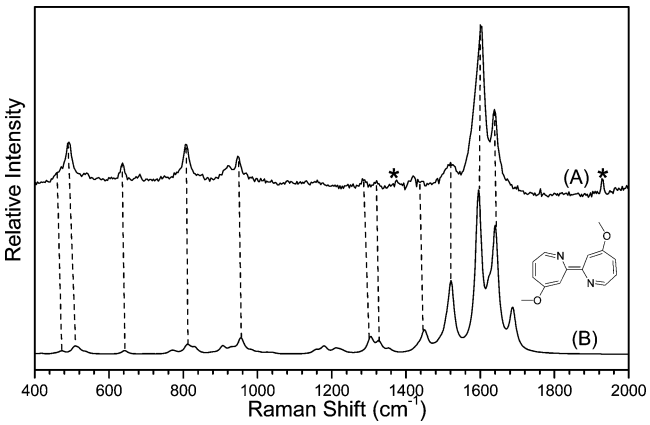

Figure 8. Comparison of (A) the experimental 50 μs TR^3 spectrum obtained after photolysis of MeOPAz in a water:acetonitrile (50:50) solution to (B) the B3LYP/6-31G* calculated normal Raman spectrum for methoxy DDA dimer **k** whose structure is displayed next the calculated spectrum. Star symbols mark solvent-subtraction artifacts, stray-light and ambient-light artifacts. See text and Table 4S for more details.

B. Assignments of the Species Observed in the TR^3 Spectra. Comparison of the experimental vibrational frequencies to those predicted from density functional theory (DFT) or *ab initio* calculations for probable intermediates has been successfully employed to identify and assign time-resolved infrared (TRIR) and time-resolved resonance Raman (TR^3) spectra to arylnitrenium ions, arylnitrenes and arylnitrene photoproducts.[18,22,26,27,34−36] A similar methodology is employed here to help assign the two kinds of species observed in the TR^3 spectra of Figures 1 and 2. Considering that the species observed in Figure 1 obtained after photolysis of NitroPAz has prominent resonance Raman bands in the 1400−1500 cm^{-1} region characteristic of N═N bond stretching vibrational modes, we examined the possibility that the species observed in Figure 1 is the 3,3′-dinitroazobenzene product, an azo compound produced by dimerization of triplet 3-nitrophenylnitrene. B3LYP/6-31G* calculations were performed to predict the total energy, the optimized geometry and vibrational frequencies for 3,3′-dinitroazobenzene. Figure 6 compares the experimental 50 μs TR^3 spectrum from Figure 1 to the B3LYP/6-31G* calculated normal Raman spectra whose relative intensities were convoluted with a Lorentzian function. Table 1S compares the experimental Raman band vibrational frequencies for the 50 μs TR^3 spectrum from Figure 1 to those predicted from the B3LYP/6-31G* calculations for 3,3′-dinitroazobenzene. Examination of Figure 6 and Table 1S shows there is good agreement between the experimental and calculated vibrational frequencies, which suggests that the species observed in Figure 1 can be tentatively assigned to the 3,3′-dinitroazobenzene. To unequivocally confirm this assignment, we prepared an authentic sample of the 3,3′-dinitroazobenzene compound using a synthetic method and compared its 341.5 nm resonance Raman spectrum to that of the experimental (50 μs post laser pulse) TR^3 spectrum (from Figure 1) as shown in Figure 6. Inspection of Figure 6 shows that the two spectra are essentially identical within experimental uncertainty and this unambiguously confirms the assignment of the species in Figure 1 to the 3,3′-dinitroazobenzene compound. This conclusion agrees with the work of Liang and Schuster[38] who demonstrated efficient formation of triplet 3-nitrophenylnitrene upon photolysis of the corresponding azide. It is not clear if the efficient intersystem crossing in this system takes place in the azide excited-state or in the singlet arylnitrene.

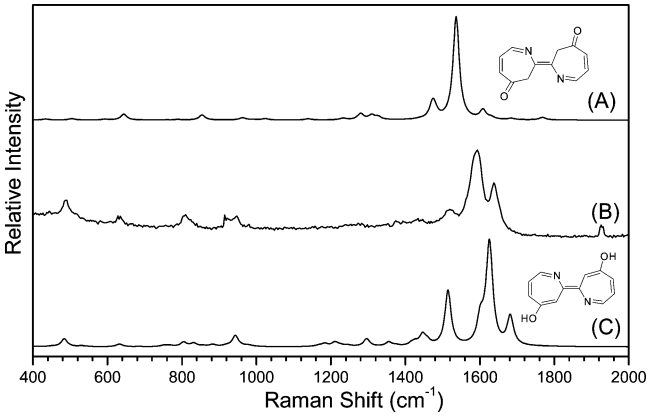

Figure 9. Comparison of (B) the experimental 50 μs TR^3 spectrum obtained after photolysis of OHPAz in a water:acetonitrile (50:50) solution to the B3LYP/6-31G* calculated normal Raman spectra for (C) hydroxy DDA dimer and (A) its corresponding ketone isomer whose structures are displayed next the calculated spectra.

From comparisons of the TR^3 spectra in Figures 1 and 2 above, the species observed in Figure 2 obtained after photolysis of PAz, OHPAz and MeOPAz were believed to have a different structure from the species observed in Figure 1, obtained after photolysis of NitroPAz. The latter spectrum was assigned to the 3,3′-dinitroazobenzene product formed from dimerization of triplet 3-nitrophenylnitrene. Figure 7 displays a comparison of the 50 μs TR^3 spectrum in Figure 2, obtained by photolysis of PAz to a resonance Raman spectrum of an authentic sample of azobenzene. These two Raman spectra are very different and clearly demonstrate that the species observed in Figure 2 after photolysis of PAz cannot be the azo compound produced from dimerization of the triplet phenylnitrene. Platz and co-workers have previously investigated the photochemistry of PAz, OHPAz and MeOPAz [2a] by using laser flash photolysis techniques with UV−vis detection and time-dependent DFT calculations and the 1,2-didehydroazepines were observed at early times. But the species observed in the TR^3 spectra of this work in Figure 2 cannot be 1,2-didehydroazepines, because they form on a time scale of tens of microseconds, significantly longer than the time scale for the formation of a 1,2-didehydroazepine, which forms with a time constant of about 1 ns. Moreover, the results of the azide concentration dependence experiments and pump laser

SCHEME 2

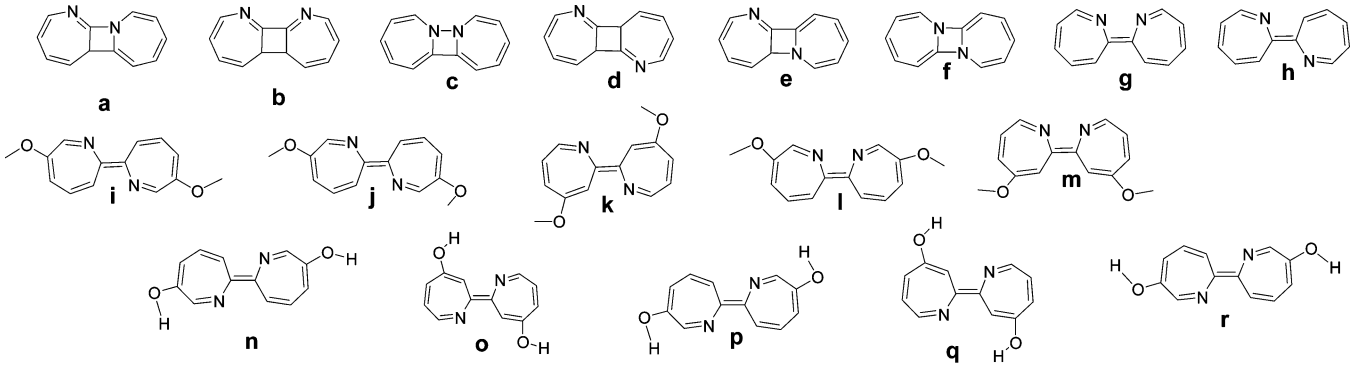

SCHEME 3

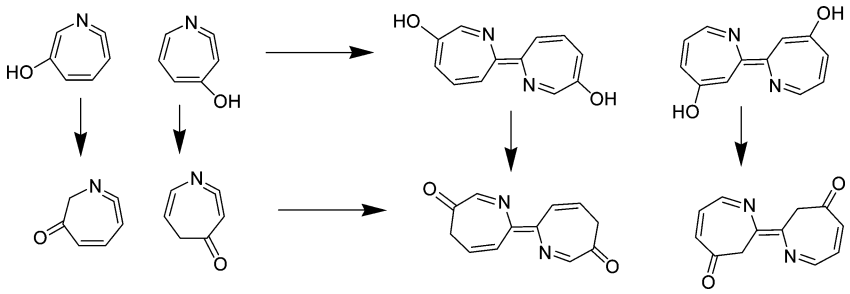

power dependence experiments clearly exclude that the species observed in Figure 2 are produced by reactions of intermediates with azide precursors. In addition, the growth of the species is not sensitive to oxygen, so this kind of species was believed to be produced by the dimerization of 1,2-didehydroazepines.

To test this possibility, B3LYP/6-31G* calculations were performed to predict the Raman spectra of several potential dimeric isomers (**a**−**h** depicted in Scheme 2) produced from 1,2-didehydroazepine, and these results were used to compare to the experimental TR[3] spectrum obtained by photolysis of PAz in mixed aqueous solvent and shown in Figure 9S of the Supporting Information. The comparison results in Figure 9S show that the calculated Raman spectra of the dimers **h** and **g** in which the carbon next to nitrogen in a 1,2-didehydroazepine connects with the double bond of its counterpart on another 1,2-didehydroazepine (referred to as the DDA dimer hereafter) agree reasonably well with the experimental one, especially the intensity and frequency pattern for the two Raman bands around 1600 cm^{-1}. So the observed species in the TR[3] spectra in Figure 2 are tentatively assigned to this kind of DDA dimer. The other reason that the anti structure DDA dimer was considered as candidate structures was inspired by Banks and co-workers[39] isolation of a stable decafluorinated analogue. Figure 7 shows a comparison of the 50 μs Raman spectrum in Figure 2 obtained by photolysis of PAz to that of the calculated spectrum for the parent DDA dimer **h**, which has an *anti* structure, and whose predicted Raman spectrum agrees best with the experimental one among all the predicted Raman spectra of the potential dimeric structures examined. Tables 2S compares the experimental and calculated Raman band vibrational frequencies in Figure 7 for the DDA dimer **h**. Examination of Figure 7 shows that the calculated Raman spectrum agrees well with the experimental spectrum for DDA dimer **h** with some moderate differences in the relative intensities that can be easily accounted for by the fact that the experimental spectra are resonantly enhanced and the calculated spectra are for normal (or non-resonance) Raman spectra. The vibrational frequencies differ only by about 7.6 cm^{-1} on average between the experimental and calculated values for the eight experimental Raman band frequencies. Figure 8 shows a comparison of the 50 μs Raman spectrum in Figure 2 (obtained by photolysis of MeOPAz) to the calculated normal Raman spectrum for the methoxy DDA dimer **k**. The calculated Raman spectrum agrees well with the experimental spectrum for DDA dimer **k**, and the vibrational frequencies differ only by about 7 cm^{-1} on average between the experimental and calculated ones for the eight experimental Raman band frequencies for **k** (see Table 4S). Several other regioisomers of methoxy DDA dimer (**i**, **j**, **l**, **m**) were also considered and their calculated Raman spectra were displayed in Figure 10S in Supporting Information. Inspection of these Raman spectra combined with Figure 8, the calculated Raman spectrum of **k** agrees best with the experimental one, so the observed species in Figure 2 obtained by photolysis of MeOPAz is tentatively assigned to methoxy DDA dimer **k**.

Figure 9 displays a comparison of the 50 μs Raman spectrum in Figure 2 (obtained after photolysis of OHPAz) to calculated normal Raman spectra for the hydroxy DDA dimer and its corresponding ketone isomer. The calculated hydroxy DDA dimer spectrum in Figure 9 displays noticeably less agreement with the experimental spectrum as compared to the corresponding agreement for the parent DDA dimer and the methoxy DDA dimer to the relevant experimental spectra in Figures 7 and 8. A particular discrepancy between the experimental and calculated spectra is that the vibrational frequency difference between the two strong bands at 1534 and 1603 cm^{-1} have a difference of 69 cm^{-1} and the strong calculated bands at 1515 and 1625 cm^{-1} have a difference of 110 cm^{-1} (see Table 3S). It is possible that the source for this more noticeable disagreement between the calculated hydroxy DDA dimer Raman spectrum and the corresponding experimental spectrum in Figure 9 is due to a fast enolization reaction to form the corresponding ketone dimer (Scheme 3, a reaction not possible for the other DDA dimers observed here).

We calculated the corresponding ketone dimer Raman spectrum with the structure shown in Figure 9, and it is different from that of the hydroxy DDA dimer Raman spectrum, which

TABLE 1: Excited States Energies and Oscillator Strengths from TD (B3LYP/6-31G*) Calculations for (A) the Parent DDA Dimer, Hydroxy DDA Dimer and Methoxy DDA Dimer, and (B) the Ketone Dimer Species That Could Be Formed from Enolization of the Hydroxy DDA Dimer

(A) Parent DDA Dimer, Hydroxy DDA Dimer and Methoxy DDA Dimer

parent DDA dimer			hydroxy DDA dimer			methoxy DDA dimer		
excited state	transition energy (nm)	oscillator strength	excited state	transition energy (nm)	oscillator strength	excited state	transition energy (nm)	oscillator strength
3	363	0.2547	3	365	0.3702	**3**	**364**	**0.5094**
4	**345**	**0.4438**	**4**	**350**	**0.2866**	**4**	**346**	**0.1926**
5	335	0.0017	5	339	0.0037	5	333	0.0086
6	298	0.0002	6	309	0.0047	6	300	0.0064
7	286	0.0192	7	292	0.0021	7	284	0.0167
8	277	0.0178	8	284	0.0135	8	282	0.0058
9	272	0.0015	9	270	0.0165	9	273	0.0702
10	263	0.0001	10	267	0.0664	10	268	0.0942
			11	260	0.3119	11	262	0.0135
			12	254	0.0516	12	257	0.0513
			13	251	0.0082	13	251	0.0529

(B) Ketone Dimer

excited state	transition energy (nm)	oscillator strength
1	555.02	0.1899
2	452.69	0.0006
3	448.72	0.0141
4	410.43	0.0104
5	358.02	0.1165
6	352.47	0.0008
7	315.44	0.002
8	309.28	0.0448

is also shown in Figure 9. The calculated spectrum for the ketone dimer also displays reasonable overall agreement with the experimental TR^3 spectrum. It is worth noting the vibrational frequency spacing between the two strong experimental bands at 1534 and 1603 cm^{-1} that have a difference of 69 cm^{-1} agrees much better with the 58 cm^{-1} spacing between the two strong calculated bands at 1478 and 1536 cm^{-1} for the ketone dimer (see Table 5S) than the 110 cm^{-1} spacing for the strong calculated bands at 1515 and 1625 cm^{-1} for the hydroxy DDA dimer (see Table 3S). Because there are a number of possible isomers for both the hydroxy DDA dimer (**n**−**r**) and the corresponding ketone species, the Raman bands in the 500−1300 cm^{-1} region can change significantly with different isomer structures, and this makes it difficult to use these to clearly distinguish between the hydroxy DDA dimer and the corresponding ketone species unless one knows which is the predominant isomer. Comparisons between the experimental Raman spectrum to the calculated normal Raman spectra predicted from other possible structures for the hydroxy DDA dimer are displayed in Figure 7S of the Supporting Information. Examination of Figure 7S shows that, although the predicted Raman bands can change substantially with isomer structure in the 500−1300 cm^{-1} region, the strong bands in the 1400−1700 cm^{-1} region display a consistent general pattern for relative intensities and vibrational frequency spacing. We therefore place more weight on the general pattern for relative intensities and vibrational frequencies for the Raman bands in the 1400−1700 cm^{-1} region to distinguish between the hydroxy DDA dimer and the corresponding ketone species. On the basis of the relative vibrational frequency patterns (like the frequency spacing pattern) in the 1400−1700 cm^{-1} region, we think it may be a ketone dimer species that is observed in the TR^3 spectra observed after photolysis of OHPAz in room temperature solutions. However, further work is needed to unambiguously assign the species observed after photolysis of OHPAz in room temperature solutions. We note that an enolization reaction to form the corresponding ketone dimer after photolysis of OHPAz could conceivably take place via several different processes (see Scheme 3). It is possible that enolization occurs after the hydroxy DDA dimer is formed. However, we see very similar spectra and dynamics in both acetonitrile and water:acetonitrile (50:50) solvents and we can rule out this pathway on the basis of our present data. An alternative enolization pathway(s) we cannot exclude is an enolization taking place during or shortly after the fast ring expansion reaction and where it is a ketone dideyhdroazepine species that undergoes dimerization to produce the corresponding ketone dimer intermediate. This type of pathway could conceivably be very fast and efficient even in normal acetontrile solvents, which have a finite water impurity. If there is a propensity for water molecules to hydrogen bond to the hydroxyl moiety, one is mostly exciting a OHPAz water cluster that subsequently forms a 3-hydroxyphenylnitrene water cluster. The hydrogen-bonded nitrene can then undergo ring expansion and enolization reactions to form the ketone didehydroazepine and its dimer. Further work using other methods sensitive to the detection of these species on the time-scale for formation and decay of the 1,2-didehydroazepine species is needed to ascertain whether or not there is enol−keto tautomerization in the intermediate produced upon photolysis of OHPAz in solvents that contain water.

Time-dependent DFT calculations were also performed to predict the electronic transitions of these DDA dimers and the ketone dimer species that could be formed from enolization of the hydroxy DDA dimer. Table 1 displays the excited-state energies and oscillator strengths in the region of 250−400 nm obtained from the TD (B3LYP/6-31G*) calculations for these three DDA dimers and the ketone dimer species. These TD DFT calculations results show that all these dimer species have strong electronic transitions around 341.5 nm and this is consistent with our observation of these species using a 341.5 nm probe wavelength in the TR^3 experiments presented in this paper.

We note that a 1,2-didehydroazepine dimer with a similar structure has been observed by Banks and co-workers[39] after

pyrolysis of azidopentafluorobenzene and this product was characterized by X-ray crystallography.

Although the species observed in the TR^3 experiments in this paper are all dimers in nature, their structures and formation mechanisms are totally different for the two basic kinds of pathways observed. The azo compound is formed from a dimerization reaction of the triplet arylnitrenes whereas the DDA dimers and maybe the ketone dimer are formed from the didehydroazepines. Fundamentally, the substituent group at the *meta* position decides the branching ratio between intersystem crossing (ISC) that results in triplet arylnitrenes and azo products and ring expansion rates of the singlet arylnitrenes to produce didehydoazepine intermediates and their subsequent reactions.

This work confirms the conclusions of earlier studies. It is clear that photolysis of NitroPAz in aqueous solution produces the corresponding triplet nitrene.[2a] The triplet nitrene will form an azo dimer, by reactions of two triplet nitrenes. In a biological milieu it is most likely that triplet 3-nitophenylnitrene will be reduced to form the corresponding aniline. The formation of azo compounds and anilines are not useful products from the point of view of photoaffinity labeling thus NitroPAz cannot be expected to efficiently label biological residues or form cross-links upon photolysis. Our previous study provided evidence for the presence of both triplet nitrene and 1,2-didehydroazepine.[2a] Evidence for the latter species was not found in this study, demonstrating the different sensitivities of different time-resolved spectroscopic techniques. If a nitro substituted didehydroazepine is formed, it can be intercepted with a potent nucleophile to form a covalently labeled adduct. Unfortunately, as the 1,2-didehydroazepine is long-lived, it can explore its environment and find a reactive partner, and that nucleophile need not be present in the original binding pocket.

This study confirms that photolysis of PAz, MeOPAz and OHPAz produce 1,2-didehydroazepines in aqueous solution. These didehydroazepines are not directly detected, but their presence is demonstrated by the formation of a characteristic dimer. The dimer likely reacts with additional molecules of 1,2-didehydroazepine to form polymeric tars.[32] As in the nitro analog, these 1,2-didehydroazepines will react only with potent nucleophiles to form adducts. Again, as the 1,2-didehydroazepine is long-lived, it can easily react with a nucleophile outside of the binding pocket of interest.

Previously, we concluded that the hydroxy substituted 1,2-didehydroazepine tautomerized to a reactive ketone. In the present study we cannot distinguish whether we are detecting a bisketone or bis enol, or both intermediates.

Conclusions

Time-resolved resonance Raman investigations of the photochemistry of PAz, OHPAz, MeOPAz and NitroPAz in solution are reported. After photolysis of these four azides in room temperature solutions, only one species was observed in TR^3 spectra for each azide, respectively. For the NitroPAz solution, the observed species was assigned to 3,3′-dinitroazobenzene, an azo compound formed from the triplet 3-nitrophenylnitrene. In phenyl azide, OHPAz and MeOPAz solutions, the species observed in TR^3 were tentatively assigned to 1,2-didehydroazepines dimer intermediates formed from 1,2-didehydroazepines.

Acknowledgment. This work was supported by grants from the Research Grants Council (RGC) of Hong Kong (HKU 7040/06P), the award of a Croucher Foundation Senior Research Fellowship (2006-07) from the Croucher Foundation and an Outstanding Researcher Award (2006) from the University of Hong Kong to DLP and in Columbus by the National Science Foundation to CMH and MSP. The Ohio Supercomputer Center is gratefully acknowledged. One of us (JW) thanks the Graduate School of the Ohio State University for a Presidential Fellowship.

Supporting Information Available: Figure 1S shows an overview of the 341.5 nm probe TR^3 spectra obtained after 266 nm photolysis of ~3 mM OHPAz in a water:acetonitrile (50:50) solution. Figure 2S shows 341.5 nm probe TR^3 spectra obtained after 266 nm photolysis of ~3 mM NitroPAz in acetonitrile. Figure 3S shows 341.5 nm probe TR^3 spectra obtained after 266 nm photolysis of ~3 mM PAz in acetonitrile. Figure 4S shows 341.5 nm probe TR^3 spectra obtained after 266 nm photolysis of ~3 mM OHPAz in acetonitrile. Figure 5S shows 341.5 nm probe TR^3 spectra obtained after 266 nm photolysis of ~3 mM OHPAz in water:acetonitrile (95:5). Figure 6S shows 341.5 nm probe TR^3 spectra obtained after 266 nm photolysis of ~3 mM MeOPAz in acetonitrile. Figure 7S shows a comparison of the experimental 50 μs TR^3 spectrum from Figure 2 obtained after photolysis of OHPAz to the B3LYP/6-31G* calculated normal Raman spectra for the hydroxy didehydroazepine dimer possible structures. Figure 8S gives the comparison of the experimental 50 μs TR^3 spectrum obtained after photolysis of OHPAz in a water:acetonitrile (50:50) solution to that obtained in acetonitrile. Figures 9S and 10S show the comparison of the experimental 50 μs TR^3 spectrum from Figure 2 obtained after photolysis of PAz and MeOPAz to the B3LYP/6-31G* calculated normal Raman spectra for the parent and 3-methoxy substituted DDA dimers, respectively. Table 1S compares the B3LYP/6-31G* calculated Raman vibrational frequencies for 3,3′-dinitroazobenzene to those observed for the 50 μs TR^3 experimental spectrum of Figure 1 obtained after photolysis of NitroPAz. Tables 2S, 3S and 4S compare the B3LYP/6-31G* calculated Raman vibrational frequencies for the DDA dimers to those observed for the 50 μs TR^3 experimental spectra of Figure 2 obtained after photolysis of PAz, OHPAz and MeOPAz in water:acetonitrile (50:50), respectively. Table 5S compares the B3LYP/6-31G* calculated Raman vibrational frequencies for ketone isomer to those observed for the 50 μs TR^3 experimental spectrum of Figure 3 obtained after photolysis of OHPAz in water:acetonitrile (50:50). Cartesian coordinates, total energies, and vibrational zero-point energies for the optimized geometry obtained from the B3LYP/6-31G* calculations for the 3,3′-dinitroazobenzene, the parent DDA dimer, the hydroxy DDA dimer and its corresponding ketone dimer and the methoxy DDA dimer investigated in this work. This material is available free of charge via the Internet at http://pubs.acs.org.

References and Notes

(1) (a) Huisgen, R.; Vossius, D.; Appl, M. *Chem. Ber.* **1958**, *91*, 1−11. (b) Huisgen, R.; Appl, M. *Chem. Ber.* **1958**, *91*, 12. (c) Doering, W.; Odum, R. A. *Tetrahedron* **1966**, *22*, 81−93.

(2) (a) Rizk, M. S.; Shi, X.; Platz, M. S. *Biochemistry* **2006**, *45*, 543−551. (b) Cline, M. R.; Mandel, S. M.; Platz, M. S. *Biochemistry* **2007**, *46*, 1981−1987.

(3) (a) Sukhai, P.; McClelland, R. A. *J. Chem. Soc., Perkin Trans.* **1996**, *2*, 1529−1530. (b) Davidse, P. A.; Kahley, M. J.; McClelland, R. A.; Novak, M. *J. Am. Chem. Soc.* **1994**, *116*, 4513. (c) McClelland, R. A. *Tetrahedron* **1996**, *52*, 6823. (d) McClelland, R. A.; Kahley, M. J.; Davidse, P. A.; Hadzialic, G. *J. Am. Chem. Soc.* **1996**, *118*, 4794.

(4) (a) Smith, P. A. S. In *Nitrenes*; Lwowski, W., Ed.; Wiley-Interscience: New York, 1970; Chapter 4. (b) Scriven, E. F. V. In *Reactive Intermediates*; Abramovich, R. A. Ed.; Plenum: New York, 1982; Vol. 2, Chapter 1.

(5) Wentrup, C. C. *Reactive Molecules*; Wiley-Interscience: New York, 1984; Chapter 4.
(6) Platz, M. S. In *Azides and Nitrenes: Reactivity and Utility*; Scriven, E. F. V., Ed.; Academic: New York, 1984; Chapter 7.
(7) *Azides and Nitrenes: Reactivity and Utility*; Scriven, E. F. V., Ed.; Academic: New York, 1984.
(8) Leyva, E.; Platz, M. S.; Persy, G.; Wirz, J. *J. Am. Chem. Soc.* **1986**, *108*, 3783−3790.
(9) Shields, C. J.; Chrisope, D. R.; Schuster, G. B.; Dixon, A. J.; Poliakoff, M.; Turner, J. J. *J. Am. Chem. Soc.* **1987**, *109*, 4723−4726.
(10) Li, Y.-Z.; Kirby, J. P.; George, M. W.; Poliakoff, M.; Schuster, G. B. *J. Am. Chem. Soc.* **1988**, *110*, 8092−8098.
(11) Platz, M. S.; Maloney, V. M. In *Kinetics and Spectroscopy of Carbenes and Biradicals*; Platz, M. S.. Ed.; Plenum: New York, 1990; pp 303−320.
(12) Schuster, G. B.; Platz, M. S. *Adv. Photochem.* **1992**, *17*, 69−143.
(13) McClelland, R. A.; Kahley, M. J.; Davidse, P. A.; Hadzialic, G. *J. Am. Chem. Soc.* **1996**, *118*, 4794−4803.
(14) Moran, R. J.; Falvey, D. E. *J. Am. Chem. Soc.* **1996**, *118*, 8965−8966.
(15) Karney, W. L.; Borden, W. T. *J. Am. Chem. Soc.* **1997**, *119*, 3347−3350.
(16) Gritsan, N. P.; Yuzawa, T.; Platz, M. S. *J. Am. Chem. Soc.* **1997**, *119*, 5059−5060.
(17) Born, R.; Burda, C.; Senn, P.; Wirz, J. *J. Am. Chem. Soc.* **1997**, *119*, 5061−5062.
(18) Srivastava, S.; Toscano, J. P.; Moran, R. J.; Falvey, D. E. *J. Am. Chem. Soc.* **1997**, *119*, 11552−11553.
(19) Nicolaides, A.; Nakayama, T.; YaMeOPAzaki, K.; Tomioka, H.; Koseki, S.; Stracener, L. L.; McMahon, R. J. *J. Am. Chem. Soc.* **1999**, *121*, 10563−10572.
(20) Gritsan, N. P.; Zhu, Z.; Hadad, C. M.; Platz, M. S. *J. Am. Chem. Soc.* **1999**, *121*, 1202−1207.
(21) Borden, W. T.; Gritsan, N. P.; Hadad, C. M.; Karney, W. L.; Kemnitz, C. R.; Platz, M. S. *Acc. Chem. Res.* **2000**, *33*, 765−771.
(22) Srivastava, S.; Ruane, P. H.; Toscano, J. P.; Sullivan, M. B.; Cramer, C. J.; Chiapperino, D.; Reed, E. C.; Falvey, D. E. *J. Am. Chem. Soc.* **2000**, *122*, 8271−8278.
(23) Nicolaides, A.; Enyo, T.; Miura, D.; Tomioka, H. *J. Am. Chem. Soc.* **2001**, *123*, 2628−2636.
(24) Gritsan, N. P.; Likhotvorik, I.; Tsao, M.-L.; Celebi, N.; Platz, M. S.; Karney, W. L.; Kemnitz, C. R.; Borden, W. T. *J. Am. Chem. Soc.* **2001**, *123*, 1425−1433.
(25) Gritsan, N. P.; Gudmundsdottir, A. D.; Tigelaar, D.; Zhu, Z.; Karney, W. L.; Hadad, C. M.; Platz, M. S. *J. Am. Chem. Soc.* **2001**, *123*, 1951−1962.
(26) Tsao, M.-L.; Gritsan, N.; James, T. R.; Platz, M. S.; Hrovat, D. A.; Borden, W. T. *J. Am. Chem. Soc.* **2003**, *125*, 9343−9358.
(27) (a) Ong, S. Y.; Zhu, P.; Poon, Y. F.; Leung, K.-H.; Fang, W. H. *Chem. Eur J.* **2002**, *8*, 2163−2171. (b) Ong, S. Y.; Zhu, P.; Leung, K. H.; Phillips, D. L. *Chem. Eur J.* **2003**, *9*, 1377−1386. (c) Chan, P. Y.; Ong, S. Y.; But, T. Y. S.; Phillips, D. L. *J. Raman. Spectrosc.* **2004**, *35*, 887.
(28) Mandel, S.; Liu, J.; Hadad, C. M.; Platz, M. S. *Phys. Chem. A* **2005**, *109*, 2816−2821.
(29) Kwok, W. M.; Chan, P. Y.; Phillips, D. L. *J. Phys. Chem. A* **2005**, *109*, 2394−2400.
(30) Wang, J.; Burdzinski, G.; Zhu, Z.; Platz, M. S.; Carra, C.; Bally, T. *J. Am. Chem. Soc.* **2007**, *129*, 8380−8388.
(31) Meijer, E. W.; Nijhuis, S.; van Vroonhoven, F. C. B. M. *J. Am. Chem. Soc.* **1988**, *110*, 7209−7210.
(32) (a) Lindsay, R. O.; Allen, C. F. H. Phenyl Azide. In *Organic Syntheses*; Horning, E. C., Ed.; Wiley and Sons: New York. 1963; Collect. Vol. III, pp 710−712. (b) Smith, P. A. S.; Hall, J. H. *J. Am. Chem. Soc.* **1962**, *84*, 480−485. (c) Di Nunno, L. *Tetrahedron* **1986**, *42*, 3913−3920. (d) Kuz'menko, V. V. *Zh. Org. Kimi* **1979**, *15*, 1108. (e) Firouzabadi, H.; Vessal, B.; Naderi, M. *Tetrahedron Lett.* **1982**, *23* (17), 1847−1850.
(33) (a) Li, Y.-L.; Leung, K. H.; Phillips, D. L. *J. Phys. Chem. A* **2001**, *105*, 10621−10625. (b) Li, Y.-L.; Chen, D.-M.; Wang, D.; Phillips, D. L. *J. Org. Chem.* **2002**, *67*, 4228−4235. (c) Li, Y.-L.; Wang, D.; Phillips, D. L. *J. Chem. Phys.* **2002**, *117*, 7931−7941. (d) Du, Y.; Ma, C.; Kwok, W. M.; Xue, J.; Phillips, D. L. *J. Org. Chem.* **2007**, *72*, 7148−7156.
(34) (a) Zhu, P.; Ong, S. Y.; Chan, P. Y.; Leung, K. H.; Phillips, D. L. *J. Am. Chem. Soc.* **2001**, *123*, 2645−2649. (b) Zhu, P.; Ong, S. Y.; Chan, P. Y.; Poon, Y. F.; Leung, K. H.; Phillips, D. L. *Chem. Eur. J.* **2001**, *7*, 4928−4936. (c) Chan, P. Y.; Ong, S. Y.; Zhu, P.; Zhao, C.; Phillips, D. L. *J. Phys. Chem. A* **2003**, *107*, 8067−8074.
(35) (a) Chan, P. Y.; Ong, S. Y.; Zhu, P.; Leung, K. H.; Phillips, D. L. *J. Org. Chem.* **2003**, *68*, 5265−5273. (b) Chan, P. Y.; Kwok, W. M.; Lam, S. K.; Chiu, P.; Phillips, D. L. *J. Am. Chem. Soc.* **2005**, *127*, 8246−8247. (c) Xue, J.; Chan, P. Y.; Du, Y.; Guo, Z.; Chung, C. W. Y.; Toy, P. H.; Phillips, D. L. *J. Phys. Chem. B* **2007**, *111*, 12676−12684.
(36) Xue, J.; Guo, Z.; Chan, P. Y.; Chu, L. M.; But, T. Y. S.; Phillips, D. L. *J. Phys. Chem. A* **2007**, *111*, 1441−1451.
(37) Frisch, M. J.; Trucks, G. W.; Schlegel, H. B.; Scuseria, G. E.; Robb, M. A.; Cheeseman, J. R.; Zakrzewski, V. G.; Montgomery, J. A., Jr.; Stratmann, R. E.; Burant, J. C.; Dapprich, S.; Millam, J. M.; Daniels, A. D.; Kudin, K. N.; Strain, M. C.; Farkas, O.; Tomasi, J.; Barone, V.; Cossi, M.; Cammi, R.; Mennucci, B.; Pomelli, C.; Adamo, C.; Clifford, S.; Ochterski, J.; Petersson, G. A.; Ayala, P. Y.; Cui, Q.; Morokuma, K.; Malick, D. K.; Rabuck, A. D.; Raghavachari, K.; Foresman, J. B.; Cioslowski, J.; Ortiz, J. V.; Baboul, A. G.; Stefanov, B. B.; Liu, G.; Liashenko, A.; Piskorz, P.; Komaromi, I.; Gomperts, R.; Martin, R. L.; Fox, D. J.; Keith, T.; Al-Laham, M. A.; Peng, C. Y.; Nanayakkara, A.; Gonzalez, C.; Challacombe, M.; Gill, P. M. W.; Johnson, B.; Chen, W.; Wong, M. W.; Andres, J. L.; Gonzalez, C.; Head-Gordon, M.; Replogle, E. S.; Pople, J. A. *Gaussian 98*; Gaussian, Inc.: Pittsburgh, PA, 1998.
(38) Liang, T.-Y.; Schuster, G. B. *Tetrahedron Lett.* **1986**, *27*, 3325−3328.
(39) Banks, R. E.; Venayak, N. *J. Chem. Soc., Chem. Commun.* **1980**, 900−901.